ELSEVIER

Thermochimica Acta 396 (2003) 119–132

thermochimica acta

www.elsevier.com/locate/tca

Formation and disappearance of the rigid amorphous fraction in semicrystalline polymers revealed from frequency dependent heat capacity

Christoph Schick*, Andreas Wurm, Alaa Mohammed[1]

Department of Physics, University of Rostock, 18051 Rostock, Germany

Received 19 January 2002; received in revised form 7 August 2002; accepted 2 October 2002

Dedicated to Professor Bernhard Wunderlich on the occasion of his 70th birthday

Abstract

For semicrystalline polymers the observed relaxation strength at glass transition is often significantly smaller than expected from the non-crystalline fraction. This observation leads to the introduction of a rigid amorphous fraction (RAF) which does not contribute to the heat of fusion or X-ray crystallinity nor to the relaxation strength at glass transition. The RAF is non-crystalline and in a glassy state at temperatures above the common glass transition. Complex heat capacity in the high frequency limit allows for the measurement of base-line heat capacity also at temperatures above the glass transition. From that the temperature and time dependence of the RAF can be obtained. For PC, PHB and syndiotactic polypropylene (sPP) it is possible to study the creation and disappearance of the RAF in situ during isothermal crystallization and on stepwise melting. If crystallization is not limited by the stability (melting point) of the crystals to be formed the total RAF is created during the isothermal crystallization. Simultaneously with the melting of the smallest crystals the RAF disappears. For these polymers vitrification and devitrification of the non-crystalline material detected as the RAF at glass transition is structural (conformational) and not temperature induced. The formation of the last growing crystals, which melt first, are responsible for the vitrification of the amorphous material around them and, consequently, by that they limit their own growth.

Keywords: Polymers; Crystallization; Glass transition; Heat capacity; TMDSC

1. Introduction

The morphology of semicrystalline polymers is often described as a lamellae stack of crystalline and non-crystalline layers [1]. This so-called “two-phase model” is successfully applied for the interpretation of X-ray diffraction as well as heat of fusion or density measurements [2]. On the other hand, it is well known that several mechanical properties as well as the relaxation strength at glass transition cannot be described by such a two-phase approach as recently discussed by Gupta [3]. From standard DSC measurements [4], dielectric spectroscopy [5–8], shear spectroscopy [8], NMR [9] and other techniques probing molecular dynamics at glass transition (α-relaxation) the measured relaxation strength is always smaller than expected from the fraction of the non-crystalline phase. The difference in mobility is caused by differ-

* Corresponding author. Fax: +49-3814981626.
E-mail address: christoph.schick@physik.uni-rostock.de (C. Schick).
[1] On leave from Physics Department, Faculty of Science, Mansoura University, Mansoura, Egypt.

0040-6031/02/$ – see front matter
PII: S0040-6031(02)00526-9

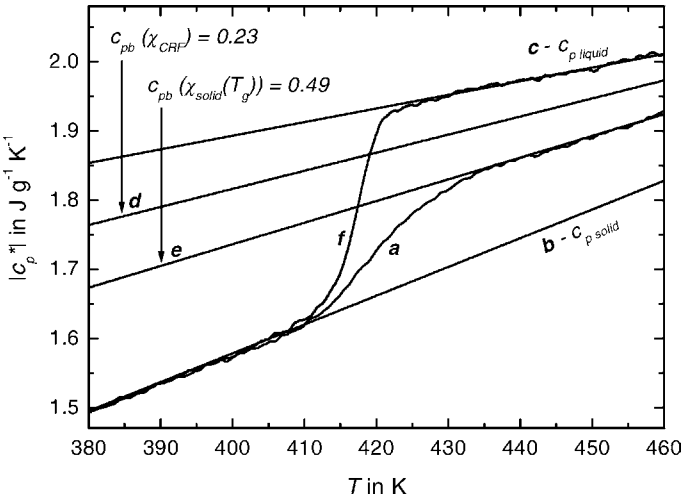

Fig. 1. TMDSC scan measurement of semicrystalline PC at underlying heating rate of 0.5 K min^{-1}, temperature amplitude 0.5 K and period 100 s, curve a. Curves b and c correspond to heat capacities from ATHAS data bank for crystalline and liquid PC, respectively. Curve d was estimated from a two-phase model, Eq. (1) and curve e from a three-phase model, Eq. (2), using $\chi_{\mathrm{solid}}(T_\mathrm{g})$. Curve f shows the measured heat capacity for the amorphous PC. TA Instruments DSC 2920.

ent conformations of the chains as detected by IR and Raman spectroscopy [10–12] or due to spatial confinement because of the neighboring lamellae. As an example the heat capacity at glass transition of amorphous and semicrystalline bisphenol-A polycarbonate (PC) is shown in Fig. 1.

According to the crystallinity of 0.23 one expects a reduction of the relaxation strength at glass transition (step height of c_p in case of calorimetric measurements) for only 23% compared to that of the totally amorphous sample. Line d represents the expected base-line heat capacity for the semicrystalline sample according to such a two-phase model and crystallinity $\chi_{\mathrm{CRF}} = 0.23$

$$c_{p\mathrm{b}}(T,t) = \chi_{\mathrm{CRF}}(T,t)c_{p\,\mathrm{crystal}}(T) + (1-\chi_{\mathrm{CRF}})(T,t)c_{p\,\mathrm{liquid}}(T) \quad (1)$$

Obviously, the reduction is much larger. It is close to 50%. To explain the disagreement between the expected values of relaxation strength as well as base-line heat capacity and the measured values, Takayanagi and coworkers [5] and Wunderlich and coworkers [4] discussed not only crystalline and non-crystalline phases in semicrystalline polymers. The non-crystalline phase has to be subdivided in one part contributing and a second one not contributing to the relaxation strength at glass transition. Furthermore, Wunderlich and coworkers distinguished between a mobile and a rigid fraction of the polymer. The rigid fraction consists of the crystalline phase and that fraction of the non-crystalline phase not contributing to the glass transition. We end up with a model distinguishing between the crystalline (CRF), the rigid amorphous (RAF) and the mobile amorphous (MAF) fractions. This model is often called "three-phase model"[2] of semicrystalline polymers. Obtaining the necessary information from the glass transition, obviously, limits the analysis to the glass transition temperature (T_g). Curve f for the initially amorphous PEEK in Fig. 2, for example, yields at T_g no rigid fraction. At T_g the sample is amorphous but at higher temperatures cold crystallization can be observed resulting in a transformation of mobile amorphous material into crystalline and rigid amorphous.

For the semicrystalline PEEK, line a in Fig. 2, a rigid fraction of about 0.55 is estimated at T_g. This is

[2] The two non-crystalline fractions (MAF, RAF) cannot be considered as different phases in thermodynamics because there is no phase transition between them. Both belong to the non-crystalline phase and can be distinguished because of differences in molecular mobility (presence or absence of the degrees of freedom typical for a liquid compared to a glass or crystal).

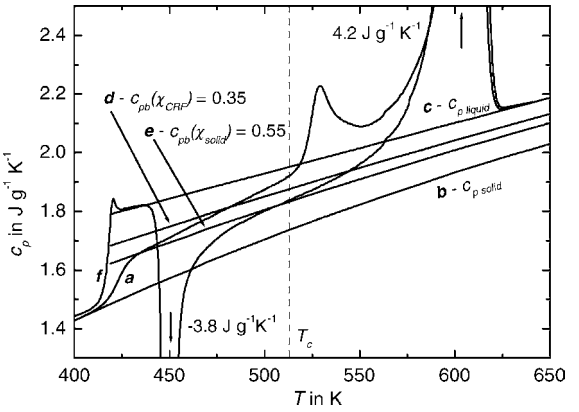

Fig. 2. DSC scan measurements of PEEK at a heating rate of 10 K min^{-1}. Curve a after isothermal crystallization for 30 min at 513 K. Curves b and c correspond to heat capacities from ATHAS data bank for crystalline and liquid PEEK, respectively. Curve d was estimated from a two-phase model, Eq. (1) and curve e from a three-phase model, Eq. (2), using $\chi_{solid}(T_g)$. Curve f shows the measured heat capacity for the initially amorphous PEEK. Perkin-Elmer Instruments Pyris Diamond DSC.

approximately twice the crystalline fraction. With this value and Eq. (2) curve e was calculated. While for the semicrystalline PC in Fig. 1 heat capacity above the glass transition is well described by Eq. (2) the heat capacity for PEEK starts to deviate from curve e just above the glass transition. The deviation may be caused by latent heats due to melting or by a broad devitrification of the RAF or both processes may appear simultaneously. Unfortunately, it is not possible to distinguish between these explanations from curves like in Fig. 2. It is still a matter of debate when the RAF disappears or when it is formed because it is not possible from such curves to obtain information about the RAF except at T_g. There may be a broad glass transition of the RAF at temperatures higher than the glass transition of the semicrystalline polymer [6,13]. Then vitrification of the amorphous material detected as the RAF at T_g occurs during cooling from the crystallization temperature down to T_g and devitrification occurs on heating in the same broad temperature interval. Lu and Cebe [14] performed annealing experiments showing that the disappearance of the RAF is somehow connected to the crystals responsible for the lowest melting endotherm in PPS. Then vitrification and devitrification of the RAF is directly coupled to crystallization and melting, respectively. In that case vitrification of the RAF occurs during crystallization and one expects significant interactions between vitrification and the crystallization process itself. The aim of this paper is to answer these questions by following the development of the RAF as a function of time during isothermal crystallization and as a function of temperature on melting. Heat capacity spectroscopy will be used to reach this goal. The present paper is an extended version of previously published work [15,16] and will partly repeat already published experimental results to verify the conclusions drawn.

2. Determination of the rigid amorphous fraction (RAF)

Differences in the molecular mobility are used to distinguish between the mobile and the RAF of a semicrystalline polymer. According to Wunderlich's definition [4] only two states are discussed. Namely, the fraction of the non-crystalline phase which contributes to the glass transition normally observed as a step change of heat capacity at temperatures slightly higher compared to the fully amorphous polymer. And a second fraction which does not contribute to the step change in heat capacity at the glass transition. This way a possibly very complex situation in respect to molecular mobility is described by only two parts. All gradients or gradual changes in molecular mobility between the crystal and the melt are neglected. Also the question if the polymer chains in the RAF have a conformation close to that of the crystal or close to that of the melt is neglected. Of course, these conformations are the reason for the differences in molecular mobility and consequently for their assignment to the RAF or to the MAF. Actually, there is no generally accepted theory of glass transition and therefore, at the moment, it is not possible to make a close relationship between conformation or changes in conformation with the contribution of particular parts of the polymer to the glass transition. Assuming the molecular processes responsible for the increase in heat capacity of a liquid compared to that of a glass are cooperative with a correlation length of about 2 nm [17], we have not discussed the behavior of single chains but we can distinguish between regions of nanometer size which do or do not contribute to the

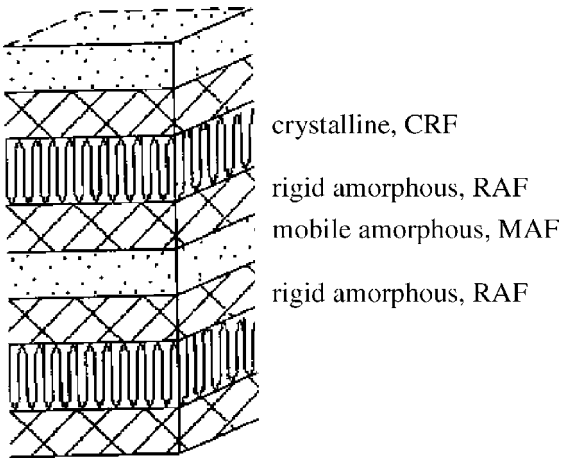

Fig. 3. Schematic sketch of the arrangement of crystalline, rigid amorphous and mobile amorphous fractions in a lamellae stack.

heat capacity step at glass transition. A very schematic sketch of such a situation is shown in Fig. 3.

Accepting such a simplified picture, heat capacity of the semicrystalline polymer can be described as a superposition of the heat capacity of the mobile fraction (χ_{MAF}) contributing and the solid fraction (χ_{solid}) not contributing to the step change of heat capacity at glass transition. For polymers heat capacity of the glassy material often equals that of the crystalline and is considered as $c_{p\,solid}$ [16]:

$$c_{pb}(T,t) = \chi_{solid}(T,t)c_{p\,solid}(T) + \chi_{MAF}(T,t)c_{p\,liquid}(T) \quad (2)$$

where $\chi_{solid} = 1 - \chi_{MAF}$ and $c_{pb}(T,t)$ is base-line heat capacity. Base-line heat capacity corresponds to the heat necessary to increase the temperature of the sample without changing crystallinity. In other words, it is the heat capacity without any contribution from latent heats.

Let us assume to be able to measure base-line heat capacity as function of temperature or time [17]. Base-line heat capacity is the superposition of the heat capacities of the different fractions as discussed above. For the three fractions, MAF, RAF, CRF, of a semicrystalline polymer we obtain

$$c_{pb}(T,t) = \chi_{MAF}(T,t)c_{p\,liquid}(T) + \chi_{RAF}(T,t)c_{p\,rigid\,amorph}(T) + \chi_{CRF}(T,t)c_{p\,crystal}(T) \quad (3)$$

and with

$$1 = \chi_{MAF} + \chi_{RAF} + \chi_{CRF} \quad (4)$$

and

$$c_{p\,solid} = c_{p\,crystal} = c_{p\,rigid\,amorph} = c_{p\,glass} \quad (5)$$

$$\chi_{RAF}(T,t) = \frac{c_{pb}(T,t) + \chi_{CRF}(T,t)[c_{p\,liquid}(T) - c_{p\,solid}(T)] - c_{p\,solid}(T)}{c_{p\,solid}(T) - c_{p\,liquid}(T)} \quad (6)$$

For most polymers $c_{p\,solid}(T)$ and $c_{p\,liquid}(T)$ are available from the ATHAS data bank [18] or can be measured. The temperature or time dependent crystallinity $\chi_{CRF}(T,t)$ can be obtained from the enthalpy changes during calorimetric measurements

$$\chi_{CRF}(T,t) = \frac{h_{liquid}(T) - h(T,t)}{h_{liquid}(T) - h_{crystal}(T)} \quad (7)$$

where $h_{liquid}(T)$ and $h_{crystal}(T)$ are the specific enthalpies of the liquid and crystalline phases, respectively, which are also available from ATHAS data bank. $h(T,t)$ is obtained from the measured enthalpy change due to crystallization or melting, for details, see [19]. The remaining task for calculation of $\chi_{RAF}(T,t)$ according to Eq. (6) is the experimental determination of base-line heat capacity $c_{pb}(T,t)$. How to obtain $c_{pb}(T,t)$ for semicrystalline polymers by means of heat capacity spectroscopy will be shown next.

3. Experimental

Different techniques can be used to measure heat capacity as a function of temperature, time, or frequency. In the present study we used temperature modulated DSC (TMDSC) and an AC calorimeter. For details of the AC calorimeter used, see [20]. TMDSC, a technique introduced in 1971 by Gobrecht et al. [21], and the necessary data treatments are described elsewhere [21–26]. If one wants to perform measurements in a broad frequency range the results from high sensitive apparatuses with different time constants like AC calorimeter, Perkin-Elmer Pyris 1 DSC and Setaram DSC 121 must be combined, for details, see [27]. For measurements at a fixed frequency of 0.01 Hz a TA

Instruments DSC 2920 was used. For the comparison of various experimental data sets, a careful temperature calibration of all instruments is necessary. The DSCs are calibrated at zero heating rate according to the GEFTA recommendation [28]. The calibration was checked in TMDSC mode with the smectic A to nematic transition of 8OCB [29,30].

The polycaprolactone (PCL) is a commercial sample from Aldrich with a molecular weight average $M_w = 55{,}700\,g\,mol^{-1}$. More details about the sample are reported in [31]. The bisphenol-A PC was obtained from General Electric (trade name LEXAN^{TM}) and was purified by dissolution in chloroform, filtering and precipitation in methanol [32,33]. The weight average molar mass and polydispersity index for the PC were obtained by gel permeation chromatography in chloroform ($M_w = 28{,}400$ g/mol and $M_w/M_n = 2.04$). The poly(3-hydroxybutyrate) (PHB) was received from the University of Cairo, Prof. A. Mansour. The syndiotactic polypropylene (sPP) ($M_w = 150{,}000$ g/mol) is a commercial product from Atofina and the PEEK Victrex 381G is from ICI. The heat capacity data for these polymers in the liquid and the crystalline state, except for PHB, are available from ATHAS data bank [18]. The heat capacities for PHB where measured outside the transition regions by TMDSC and interpolated for the liquid state and extrapolated for the solid state [17].

The measured heat capacity is the superposition of base-line and excess heat capacities. For measurements through phase transitions it is not possible to distinguish them. In some cases base-line heat capacity can be obtained from model calculations. For low molecular mass compounds where base-line heat capacity can be measured outside the transition region the change in the transition region can be estimated from the progress of the phase transition (sigmoidal base-line for peak integration). But this is only possible for two-phase systems. As soon as a third fraction is present the information available from a single heat capacity curve is not enough to distinguish three fractions straightforward. Assuming a certain coupling between the RAF and the CRF allows to solve the problem in an iterative way [34]. But the validity of the assumption must be independently checked and the experimental data must be of high accuracy. Therefore a direct measurement of base-line heat capacity is favorable.

To avoid latent heat contributions it would be nice to measure at constant temperature. But for the measurement of heat capacity changes in temperature are a prerequisite. On the other hand, it is known that high molecular mass polymers need a super-cooling in the order of 10 K for crystallization. Therefore quasi-isothermal experiments with small temperature amplitudes, as illustrated in Fig. 4, should allow to measure base-line heat capacity if the isothermal period is long enough to finish all crystallizations, re-organization or re-crystallization in the crystallization or melting region of a polymer.

It was shown by Okazaki and Wunderlich [35] that also under quasi-isothermal conditions contributions due to latent heats appear in the measured heat

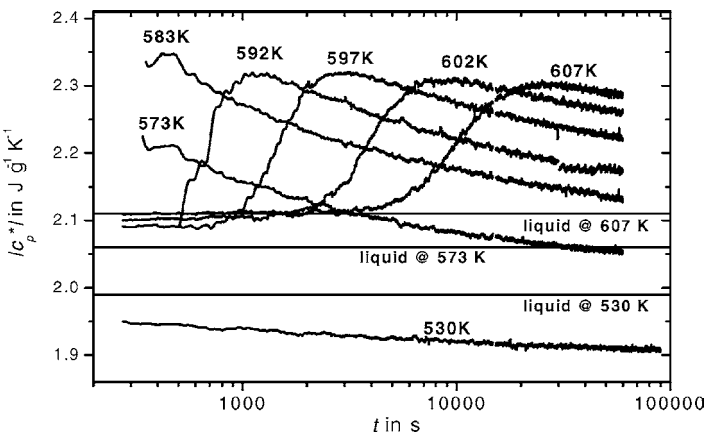

Fig. 4. Modulus of complex heat capacity at quasi-isothermal crystallization of PEEK at different temperatures. Temperature amplitude 1 K and period 200 s. Perkin-Elmer Instruments Pyris Diamond DSC.

capacity. The heat capacity values above the liquid heat capacity in Fig. 4 cannot be explained at all without contributions from latent heat. But also at long times heat capacity is larger than base-line heat capacity from Eq. (1). Consequently, these quasi-isothermal measurements do not allow to measure base-line heat capacity during the crystallization of PEEK.

A more detailed study of the excess heat capacity under quasi-isothermal conditions yields a frequency dependence of the excess heat capacity [27,36–38]. The origin of the excess heat capacity during quasi-isothermal measurements and its frequency dependence is not yet understood. Probably, the molecular processes involved are related to the surface of the polymer crystallites and often the term reversing melting [35] is used. For polymers showing a sliding diffusion in the crystallites (α-relaxation in case of polyethylene or polyethylene oxide), large contributions to reversing melting are due to surface melting [38]. For other semicrystalline polymers processes at the lateral surfaces may be responsible for the process of reversing melting and the corresponding excess heat capacity [39,40].

From glass transition, it is well known and generally accepted to describe heat capacity by complex numbers. The typical frequency dependence as known from other dynamic measurements is observed—a sigmoid step in real and a peak in imaginary part of heat capacity [21,41,42]. A similar frequency dependence of heat capacity of semicrystalline polymers was observed outside the glass transition range [27,36,38]. These observations are related to the occurrence of the excess heat capacity which occurs in a rather wide temperature range between glass transition and melting temperature. In order to obtain information about the characteristic time scale of the molecular process related to excess heat capacity we have studied the frequency dependence of complex heat capacity during quasi-isothermal crystallization for PCL, sPP, PHB and PC, see Fig. 5. To extend the frequency range available with TMDSC (10^{-5} to 10^{-1} Hz) AC calorimetric measurements were performed at a frequency of 1 Hz [20]. For PCL, a mean relaxation time in the order of a few seconds can be estimated for the process at 328 K while for sPP at 363 K it is in the order of 500 s. For PC and PHB we did not observe any frequency dependence after isothermal crystallization at 457 and 296 K, respectively. For these polymers, a frequency dependent excess heat capacity was only observed at higher temperatures in the melting range.

The frequency range available is still not broad enough for a detailed discussion of the curve shape, see Fig. 5. But from the curves one expects to measure base-line heat capacity without contributions due to

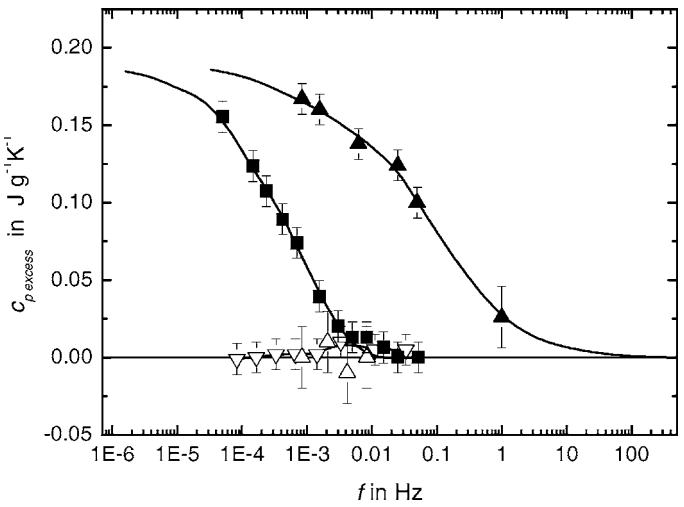

Fig. 5. Excess heat capacity during isothermal crystallization of PCL (▲) after 120,000 s at 328 K, of sPP (■) after 10,000 s at 363 K, of PC (▽) after 900,000 s at 457 K, and of PHB (△) after 100,000 s at 296 K as a function of modulation frequency. Perkin-Elmer Instruments Pyris 1 DSC, Setaram DSC 121 and AC calorimeter.

reversing melting at high frequencies. For PCL high means higher than about 100 Hz which is outside the accessible frequency range for our experimental techniques. But for sPP, PHB, and PC measurements at frequencies of about 0.01 Hz, which is inside the frequency range of TMDSC, allow for the measurement of the high frequency asymptotic value.

In general, the frequency dependence of the excess heat capacity as shown in Fig. 5 always allows for the measurement of base-line heat capacity at sufficiently high frequencies. Whether or not for a particular polymer the high frequency limit can be reached by the calorimeters available and whether or not the curve is shifted along the frequency axis with temperature has to be checked for each single experiment. It is still an open question if a time–temperature superposition is possible for the frequency dependent excess heat capacity.

For polymers like sPP, PC, and PHB base-line heat capacity is experimentally accessible in the temperature range between conventional glass transition and melting. For these semicrystalline polymers, it is therefore possible to study the formation and the disappearance of the RAF according to Eq. (6).

4. Results

In Fig. 6, the time evolution of heat capacity during isothermal crystallization of PC at 457 K is shown. To check whether or not base-line heat capacity is measured the frequency dependence was studied at the end of crystallization, see Fig. 5. No frequency dependence of measured heat capacity can be seen indicating the absence of reversing melting and that base-line heat capacity was obtained.

To answer the question if the RAF was formed isothermally during the crystallization process or on cooling from the crystallization temperature to the glass transition the measured base-line heat capacity at the end of the measurement was first compared with the expected values according to a two-phase model, Eq. (1), curve d. Base-line heat capacity is assumed to be the superposition of the heat capacities of the crystalline and the non-crystalline fraction. If the non-crystalline material detected as the RAF at T_g vitrifies on cooling and not during isothermal crystallization one expects an agreement between Eq. (1) and the measured base-line heat capacity during and at the end of the isothermal crystallization. As can be seen in Fig. 6, measured heat capacity becomes significantly

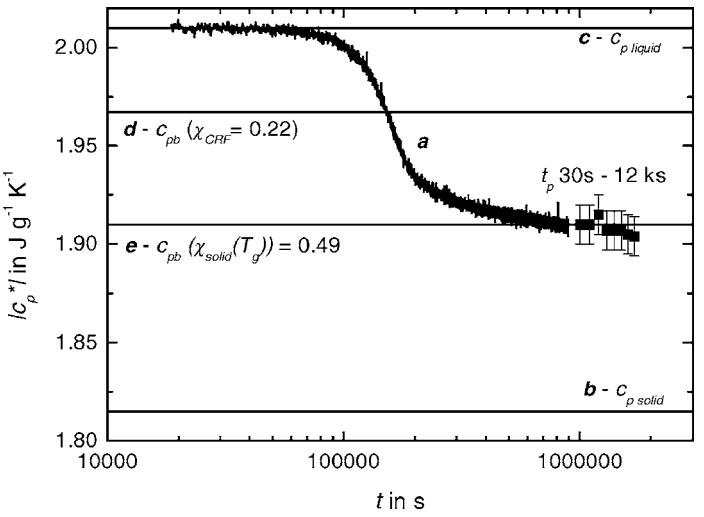

Fig. 6. Time evolution of heat capacity during quasi-isothermal crystallization of PC at 457 K, temperature amplitude 0.5 K and period 100 s, curve a. Curves b and c correspond to crystalline and liquid heat capacities from ATHAS data bank, respectively. Curve d was estimated from a two-phase model, Eq. (1) and curve e from a three-phase model, Eq. (2), using $\chi_{solid}(T_g)$ from Δc_p. The squares represent measurements at modulation periods ranging from 30 to 12,000 s. TA Instruments DSC 2920, Perkin-Elmer Instruments Pyris 1 DSC, Setaram DSC 121.

smaller than curve d—indicating the occurrence of a significant RAF at the end of the isothermal crystallization process. Next, we compare the measured base-line heat capacity with the expected value according to a three-phase model, Eq. (2), curve e. Let us now assume vitrification of the non-crystalline material detected as the RAF at T_g occurs during the isothermal crystallization and nothing happens on cooling from the crystallization temperature to the glass transition. Then we expect an agreement between the measured heat capacity and the heat capacity from Eq. (2) using the MAF determined at T_g from the step height of heat capacity at the glass transition. Line e in Fig. 6 was accordingly estimated. The agreement is perfect within the accuracy of the measurement. For PC we conclude that the total RAF was established (vitrified) during the isothermal crystallization. No additional vitrification occurs on cooling from the crystallization temperature (457 K) down to the glass transition at 420 K.

For polymers crystallizing faster than PC it is difficult to follow isothermal crystallization by TMDSC at the temperature of maximum crystallization rate as we did for PC. We have either to choose temperatures closer to the melting or closer to the glass transition temperature to reduce crystallization rate to a reliable value. To choose crystallization temperatures close to the melting temperature is often not possible because of large excess heat capacities at typical TMDSC frequencies, see Fig. 4 for PEEK. Furthermore, a comparison between data obtained at such high temperatures with that obtained at T_g is problematic because of possible changes in morphology on cooling. Choosing crystallization temperatures close to T_g, on the other hand, requires polymers which can be quenched without crystallization on cooling from the melt. PHB and sPP are polymers where this can be easily done. The result from quasi-isothermal crystallization of PHB at 296 K, what is close to the glass transition, is shown in Fig. 7.

Base-line heat capacity was measured as a function of time and compared with the predictions of Eqs. (1) and (2). As for PC the RAF in PHB is established during the quasi-isothermal crystallization as can be seen from the agreement of line e with the measured heat capacity at the end of the crystallization process. Because of the faster crystallization rate compared to PC we were able to measure the exothermic effect due to the crystallization process. The Pyris 1 DSC allows for a quantitative measurement over 17 h also the maximum of the heat flow rate was less than 40 μW. From the integral we obtain the enthalpy change, $h(t)$, and with Eq. (7) the CRF as a function of time.

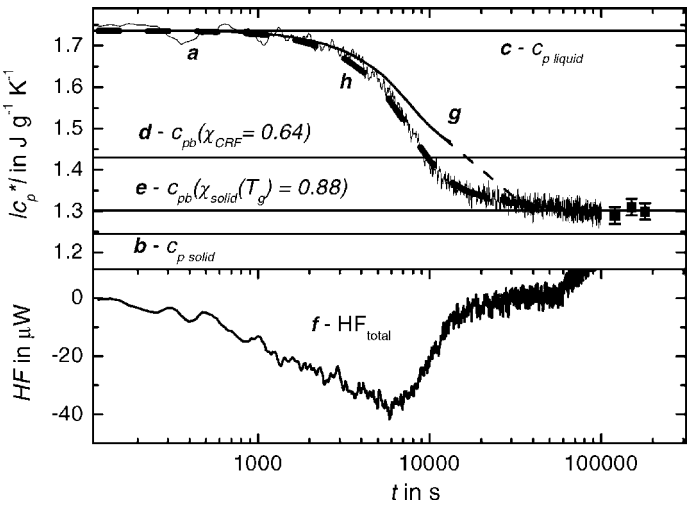

Fig. 7. Time evolution of heat capacity during quasi-isothermal crystallization of PHB at 296 K, temperature amplitude 0.4 K and period 100 s, curve a, thin line. Curves b and c correspond to solid and liquid heat capacities, respectively. Curve d was estimated from a two-phase model, Eq. (1) and curve e from a three-phase model, Eq. (2), using $\chi_{solid}(T_g)$ from Δc_p. The squares represent measurements at modulation periods ranging from 240 to 1200 s. Curve f shows the exothermal effect in the total heat flow and curves g and h, thick dashed line, the expected values from model calculations, see text. Perkin-Elmer Instruments Pyris 1 DSC.

The time dependence of base-line heat capacity can be determined from

$$c_{pb}(t) = c_{p\,\mathrm{liquid}} - \frac{\chi_{\mathrm{CRF}}(t)}{\chi_{\mathrm{CRF}}(\infty)}(c_{p\,\mathrm{liquid}} - c_{pb}(\infty)) \quad (8)$$

The calculation can be performed for two cases: (i) the RAF is formed during the whole crystallization process or (ii) first the crystalline morphology is build up during main crystallization and in a second step, e.g. during secondary crystallization at longer times, the RAF is formed. Then during main crystallization no or only a little RAF should be present. The situation (ii) should be described by Eq. (8) where $c_{pb}(\infty)$ is equal to the value from Eq. (1), line d, taking into account liquid and crystalline material only. Curve g in Fig. 7 shows the result. Also the behavior at longer times (>10,000 s) is not known, the result during main crystallization is not in agreement with the measured curve. To calculate $c_p(t)$ according to assumption (i) $c_{pb}(\infty)$ is equal to the value from Eq. (2), line e. Here it is assumed that the RAF is formed during or just after the formation of the lamella. Curve h in Fig. 7 shows the result. The agreement is perfect within the scatter of the experimental points.

For sPP quasi-isothermal crystallization was performed close to the glass transition at 280 K and closer to the melting temperature at 363 K. Fig. 8 shows the result for crystallization close to the glass transition. Despite the fact that the quality of the measurement is not as good as for PC and PHB the behavior is very similar. All or at least most of the RAF is formed during the isothermal crystallization.

For crystallization at 363 K the situation changes. First of all it is not possible to follow crystallization with time because it is too fast. In Fig. 9, the frequency dependence of the heat capacity after 3 h isothermal crystallization at 363 K is shown. For frequencies higher than 3 mHz no frequency dependence is observed. At these frequencies base-line heat capacity is measured. The value is again lower than expected from a two-phase model, Eq. (1), but it is significantly above the value for the three-phase model, Eq. (2), taking into account the RAF detected at T_g.

There must be further vitrification of amorphous material on cooling from 363 K to the glass transition at 270 K. To find out what is the reason for this vitrification we performed TMDSC scan measurements on cooling from 363 to 230 K and successive heating to the melt at 420 K. The heat capacity data obtained on cooling and heating in the temperature range 363–230–363 K are the same within the thickness of the line in Fig. 10.

In the temperature range between the crystallization temperature and 320 K significant deviations from line e are observed. Near the crystallization temperature heat capacity is close to the value expected from

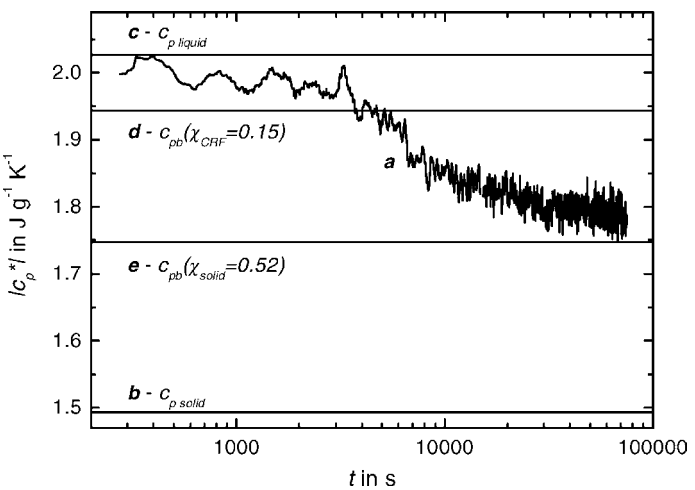

Fig. 8. Time evolution of heat capacity during quasi-isothermal crystallization of sPP at 280 K, just above T_g. Temperature amplitude 0.5 K and period 120 s, curve a. Curves b and c correspond to solid and liquid heat capacities, respectively. Curve d was estimated from a two-phase model, Eq. (1) and curve e from a three-phase model, Eq. (2), using $\chi_{\mathrm{solid}}(T_g)$ from Δc_p. Perkin-Elmer Instruments DSC2.

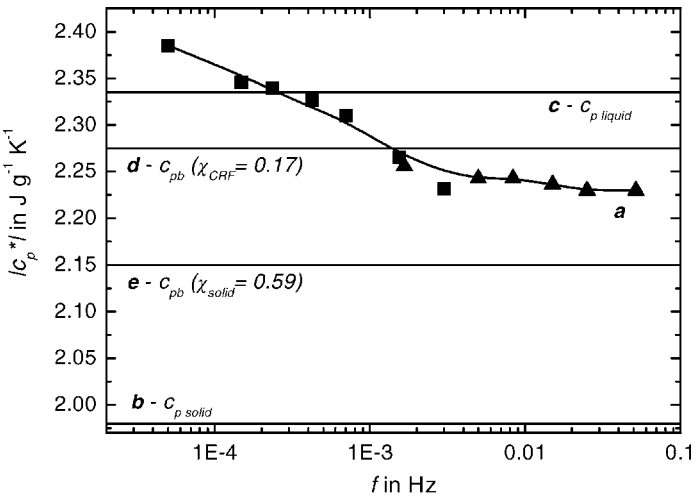

Fig. 9. Modulus of specific complex heat capacity of sPP after crystallization at 363 K for 3 h as a function of frequency. Quasi-isothermal rectangular multi-frequency temperature–time profile [43] with period 600 s, triangles, Perkin-Elmer Instruments Pyris 1 DSC, and 20,000 s, squares, Setaram DSC 121. Temperature amplitude 1 K.

a two-phase model, line d. Devitrification and vitrification occurs in a broad temperature range of about 40 K. If this is due to a broad glass transition one would not expect latent heats in this temperature range. But also below 363 K the total heat capacity, dashed line f in Fig. 10, is significantly higher than the modulus of complex heat capacity, line a in Fig. 10. This indicates latent heats because of crystallization on cooling and melting on heating. For sPP part of the RAF devitrifies on heating below the crystallization temperature (363 K). Here devitrification and melting are superimposed over a broad temperature range. Possible explanations will be discussed below.

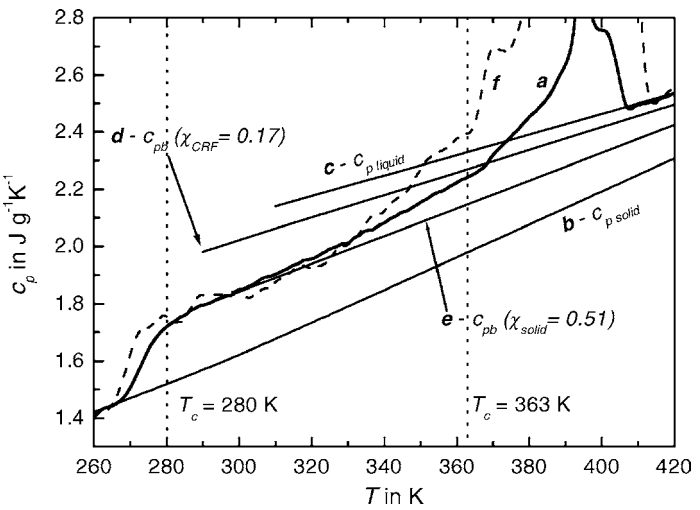

Fig. 10. TMDSC scan measurement of sPP after crystallization at 363 K for 3 h at underlying heating rate 1 K min^{-1}, temperature amplitude 0.4 K and period 60 s, curve a, thick line. Curves b and c correspond to heat capacities for solid and liquid sPP and curves d and e to expected heat capacities from a two- and a three-phase model, respectively. Curve f, dashed line, shows the total heat capacity. The vertical dotted line shows the crystallization temperature. Perkin-Elmer Instruments DSC 2.

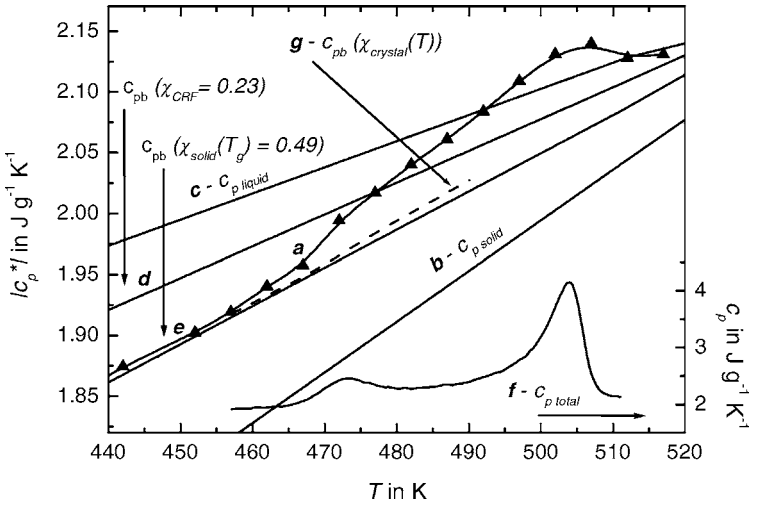

Fig. 11. Melting region of PC. Quasi-isothermal TMDSC measurements on stepwise increase in temperatures taken after 15 min (▲) at $t_p = 100$ s. Curves b and c correspond to heat capacities for solid and liquid PC, respectively. Curve d was estimated from a two-phase model, Eq. (1) and curves e and g from a three-phase model, Eq. (2), using data from T_g or temperature dependent crystallinity, respectively. Curve f shows the total heat capacity at underlying heating rate 0.5 K min^{-1}. TA Instruments DSC 2920.

For PC and PHB, where all RAF vitrifies at the crystallization temperature, the question arises at what temperature the RAF devitrifies on heating? Is devitrification smeared over a broad temperature interval? Does it occur before the crystals melt? Or is devitrification of the RAF part of the main melting? To answer these questions heat capacity was measured on stepwise heating and compared with expected base-line heat capacities, see Figs. 11 and 12 for PC and PHB, respectively. To avoid contributions from irreversible

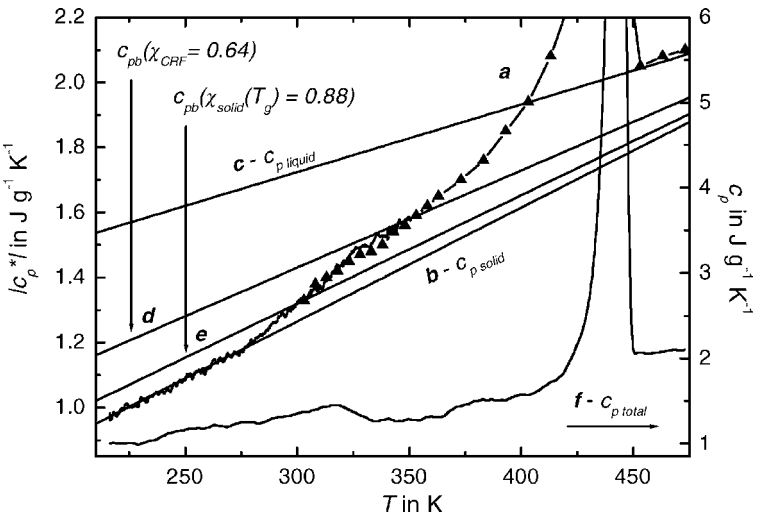

Fig. 12. TMDSC scan measurement (lines) of semicrystalline PHB at underlying heating rate of 1 K min^{-1}, temperature amplitude 0.4 K and period 60 s, curve a. Curves b and c correspond to heat capacities for solid and liquid PHB, respectively. Curve d was estimated from a two-phase model, Eq. (1) and curve e from a three-phase model, Eq. (2) using data from T_g. The triangles show heat capacities from quasi-isothermal TMDSC measurements on stepwise increasing temperatures. The data were taken after 30 min. Curve f shows the total heat capacity. Perkin-Elmer Instruments Pyris 1 DSC.

melting to the measured complex heat capacity quasi-isothermal measurements at stepwise increasing temperatures were performed, see [44] for details.

The heat capacity measured at stepwise heating in the melting region of PC, Fig. 11, curve a, shows deviations from base-line heat capacity, line e, in the temperature range above 460 K. At the lowest endotherm, between 460 and 485 K, a pronounced increase in heat capacity is observed. The heat capacity starts to deviate from the base-line heat capacity obtained from a three-phase model including RAF, Eq. (2), curve e, and around 480 K it is close to the base-line heat capacity obtained from a two-phase model, Eq. (1), curves d and g. In Eq. (1) only crystalline and liquid material is taken into account. The increase in heat capacity cannot be explained by the decrease of crystallinity due to the lowest melting endotherm between 465 and 485 K. The expected increase due to the change in crystallinity at the lowest endotherm corresponds to the difference between curve g, which was calculated from Eq. (1) assuming temperature dependent crystallinity, and curve d assuming constant crystallinity. At 480 K the difference is $0.01\,J\,g^{-1}\,K^{-1}$ only. The observed step in heat capacity is about 5 times larger. At about 490 K heat capacity becomes larger than liquid heat capacity because of excess heat capacity, see Section 5.

Basically, the same behavior as for the PC is observed for PHB on heating. Again, at the lowest endotherm around 320 K a second step in heat capacity towards the expected value from the two-phase model is observed. Because PHB crystallizes fast, the isothermal crystallization was performed close to the glass transition to be able to follow the crystallization process. Consequently, pre-melting is not well separated from glass transition in temperature.

5. Discussion

For sPP, PC, and PHB a significant RAF can be determined from the step of heat capacity at the glass transition. Taking into account the crystalline, the rigid amorphous and the mobile amorphous material information about the fractions of different molecular mobility can be obtained. For PC after 11 days crystallization at 457 K crystallinity was 0.23, RAF was 0.26 and mobile amorphous fraction was 0.51. For PHB after crystallization at 296 K for 28 h, the values were 0.64, 0.22, 0.12 and for sPP after crystallization at 280 K for 20 h 0.15, 0.37, 0.48, respectively. From the TMDSC scan measurements no reversible melting can be detected for these semicrystalline polymers at temperatures above glass transition and below the lowest endotherm. While PC crystallizes extremely slow, PHB crystallizes reasonably fast like PET, PEEK, PEN, and high degrees of crystallinity are reached. We do not know why these polymers do not show excess heat capacities under the given experimental conditions, indicating the absence of reversing melting, while other polymers like PCL, PET, PEN, and PEEK show large excess heat capacities [35,45,46].

The absence of excess heat capacities in a temperature range suitable for crystallization experiments allows us to study base-line heat capacity as a function of time and to compare measured with expected values, see Figs. 6–8. For PC, PHB and sPP at low crystallization temperatures the measured heat capacity becomes significantly smaller than base-line heat capacity expected from a two-phase model, Eq. (1). For these polymers a significant portion of the RAF is formed during the isothermal crystallization process. Furthermore, a perfect match between the measured heat capacity at the end of crystallization and the expected base-line heat capacity from a “three-phase model”, Eq. (2), can be seen. Because in Figs. 6–8, line e, was obtained with the RAF determined from the heat capacity increment at T_g, there are no indications for changes in the amount of the RAF on cooling from the crystallization temperature to the glass transition. In other words, the whole RAF, detected at T_g, was established during the quasi-isothermal crystallization. From these observations we can conclude that, at least for PC, there is no broad glass transition of the RAF somewhere in between crystallization temperature and T_g. Consequently, vitrification of the RAF results from the crystallization process itself and prevent further crystallization. For PC and PHB, at the crystallization temperatures studied, the low degree of crystallinity seems to be caused by the formation of the RAF during crystallization. Vitrification of the RAF is the result of morphological changes and not due to cooling below a second glass transition temperature. This is in agreement with the observations of Lu and Cebe [14] for PPS but does not support the view of Song and Hourston [13] and Huo and Cebe

[6] considering a broad glass transition of the RAF for PET and PEEK, respectively.

For sPP at higher crystallization temperatures the situation is not simple. As can be seen from Fig. 10, the low frequency asymptotic value of the specific heat capacity after isothermal crystallization at 363 K is only a little below the expected value from a two-phase model, line d, Eq. (1), and significantly larger than the expected value obtained from the heat capacity increment at glass transition, line e, Eqs. (2) and (7). For sPP, a significant part of the RAF detected at the glass transition is still mobile at the end of the isothermal crystallization at 363 K and vitrifies on cooling. There are significant changes in heat capacity between crystallization temperature and the conventional glass transition. But the latent heat observed in this temperature range indicates simultaneous changes in morphology. The sequence length distribution of the crystallizable sequences may be responsible for this behavior. For polymers where the crystallization is controlled by tacticity or distribution of non-crystallizable co-units along the chain the size of possible crystals may be defined by the length of the crystallizable sequences. Therefore, for crystallization temperatures above the melting temperature of the smallest crystals (shortest sequences), these crystals cannot be formed. On cooling, as soon as temperature is below the corresponding crystallization temperature, the small crystals are formed. The formation of such small crystals results in the reduction of the molecular mobility of the surrounding melt and consequently in the vitrification of the amorphous material which is detected as the RAF at T_g. For sPP, contrary to PC and PHB, the RAF mainly vitrifies on cooling from the crystallization temperature (363 K) to the glass transition within ca. 40 K. Consequently, crystallization cannot be limited by the vitrification of the melt surrounding the growing crystals. For sPP other reasons must be responsible for the very low degree of crystallinity finally reached. It may be the length distribution of crystallizable sequences of the necessary stereo-regularity which limits crystallization of sPP.

6. Conclusion

For PC, sPP and PHB the asymptotic value of heat capacity at high frequencies can be measured by TMDSC during crystallization. This allows to measure base-line heat capacity and to study the formation of the RAF. For PC, PHB and sPP the RAF is established during isothermal crystallization. Devitrification of the RAF occurs at the lowest endotherm. The immobilization of the amorphous material around less perfect crystals, which are formed during isothermal crystallization, results in the vitrification of the RAF during crystallization and in its devitrification during melting. For sPP, crystallized at 363 K, only a small fraction of the RAF detected at the glass transition is vitrified during isothermal crystallization. These differences regarding the vitrification of the RAF indicate differences in the crystallization process. While for PC, PHB and sPP at 280 K crystallization is limited by the vitrification of the melt surrounding the growing crystals for sPP at 363 K, other mechanisms must be responsible for the low degree of crystallinity reached. The length distribution of the crystallizable sequences must be considered. In any case, vitrification of the RAF results from the crystallization process itself. Vitrification of the RAF is the result of morphological changes and not due to cooling below a sometimes assumed second glass transition temperature in the semicrystalline polymers.

Acknowledgements

We are thankful to Prof. H. Marand, Blacksburg, VA, for supplying the PC sample and to Prof. A. Mansour, Cairo, for supplying the PHB sample and to both for stimulating discussions. This research was supported by the European Commission (grant IC15CT96-0821), the German Science Foundation (grant DFG Schi-331/5) (AW) and the Government of Egypt (AM). We acknowledge support by Perkin-Elmer Instruments and TA Instruments.

References

[1] G. Strobl, The Physics of Polymers, Springer, Berlin, 1996.
[2] V. Sharma, P. Desai, A.S. Abhiraman, J. Appl. Polym. Sci. 65 (1997) 2603.
[3] V.B. Gupta, J. Appl. Polym. Sci. 83 (2002) 586.
[4] H. Suzuki, J. Grebowicz, B. Wunderlich, Makromol. Chem. 186 (1985) 1109.
[5] Y. Ishida, K. Yamafuji, H. Ito, M. Takayanagi, Kolloid Z. Z. Polym. 184 (1962) 97.

[6] P. Huo, P. Cebe, Macromolecules 25 (1992) 902.
[7] K. Nogales, T.A. Ezquerra, F. Batallan, B. Frick, E. Lopez-Cabarcos, F.J. Balta-Calleja, Macromolecules 32 (1999) 2301.
[8] C. Schick, J. Dobbertin, M. Potter, H. Dehne, A. Hensel, A. Wurm, A.M. Ghoneim, S. Weyer, J. Therm. Anal. 49 (1997) 499.
[9] W. Gabrielse, H.A. Gaur, F.C. Feyen, W.S. Veeman, Macromolecules 27 (1994) 5811.
[10] K.C. Cole, A. Ajji, E. Pellerin, Macromolecules 35 (2002) 770.
[11] G. Strobl, W. Hagedorn, J. Polym. Sci. B 16 (1978) 1181.
[12] M. Glotin, L. Mandelkern, Colloid Polym. Sci. 260 (1982) 182.
[13] M. Song, D.J. Hourston, J. Therm. Anal. 54 (1998) 651.
[14] S.X. Lu, P. Cebe, Polymer 37 (1996) 4857.
[15] C. Schick, A. Wurm, A. Mohammed, Thermochim. Acta 392/393 (2002) 303–313.
[16] C. Schick, A. Wurm, A. Mohammed, Colloid Polym. Sci. 279 (2001) 800.
[17] E. Donth, The Glass Transition, Springer, Berlin, 2001.
[18] B. Wunderlich, Pure Appl. Chem. 67 (1995) 1019. http://web.utk.edu/~athas/databank/intro.html.
[19] V.B.F. Mathot, Calorimetry and Thermal Analysis, Carl Hanser, Munich, Chapter 5.2, 1994.
[20] A.A. Minakov, Yu. Bugoslavsky, C. Schick, Thermochim. Acta 317 (1998) 117.
[21] H. Gobrecht, K. Hamann, G. Willers, J. Phys. E 4 (1971) 21.
[22] B. Wunderlich, Y.M. Jin, A. Boller, Thermochim. Acta 238 (1994) 277.
[23] M. Reading, Trends Polym. Sci. 8 (1993) 248.
[24] J.E.K. Schawe, Thermochim. Acta 260 (1995) 1.
[25] M. Merzlyakov, C. Schick, Thermochim. Acta 330 (1999) 55 and 65.
[26] S. Weyer, A. Hensel, C. Schick, Thermochim. Acta 304–305 (1997) 267.
[27] M. Merzlyakov, A. Wurm, M. Zorzut, C. Schick, J. Macromol. Sci.-Phys. B 38 (1999) 1045.
[28] S.M. Sarge, W. Hemminger, E. Gmelin, G.W.H. Höhne, H.K. Cammenga, W. Eysel, J. Therm. Anal. 49 (1997) 1125.
[29] A. Hensel, C. Schick, Thermochim. Acta 304–305 (1997) 229.
[30] C. Schick, U. Jonsson, T. Vassiliev, A.A. Minakov, J.E.K. Schawe, R. Scherrenberg, D. Lörinczy, Thermochim. Acta 347 (2000) 53.
[31] P. Skoglund, A. Fransson, J. Appl. Polym. Sci. 61 (1996) 2455.
[32] S. Sohn, A. Alizadeh, H. Marand, Polymer 41 (2000) 8879.
[33] A. Alizadeh, S. Sohn, J. Quinn, H. Marand, L. Shank, H.D. Iler, Macromolecules 34 (2001) 4066.
[34] M. Alsleben, C. Schick, Thermochim. Acta 238 (1994) 203.
[35] I. Okazaki, B. Wunderlich, Macromolecules 30 (1997) 1758.
[36] Y. Saruyama, Thermochim. Acta 305 (1997) 171.
[37] A. Toda, C. Tomita, M. Hikosaka, Y. Saruyama, Thermochim. Acta 324 (1998) 95.
[38] T. Albrecht, S. Armbruster, S. Keller, G. Strobl, Macromolecules 34 (2001) 8456.
[39] C. Schick, M. Merzlyakov, A.A. Minakov, A. Wurm, J. Therm. Anal. Cal. 59 (2000) 279.
[40] R. Androsch, B. Wunderlich, Macromolecules 34 (2001) 5950.
[41] N.O. Birge, S.R. Nagel, Phys. Rev. Lett. 54 (1985) 2674.
[42] S. Weyer, A. Hensel, C. Schick, Thermochim. Acta 304–305 (1997) 251.
[43] M. Merzlyakov, C. Schick, Thermochim. Acta 377 (2001) 193.
[44] A. Wurm, C. Schick, Colloid Polym. Sci., DOI 10.1007/s00396-002-0746-4.
[45] M. Pyda, B. Wunderlich, J. Polym. Sci. B 38 (2000) 622.
[46] A. Wurm, M. Merzlyakov, C. Schick, J. Macromol. Sci.-Phys. B 38 (1999) 693.